HHS Public Access

Author manuscript

NMR Biomed. Author manuscript; available in PMC 2019 September 01.

Published in final edited form as:

NMR Biomed. 2018 September ; 31(9): e3948. doi:10.1002/nbm.3948.

Feasibility of Quantitative Ultrashort Echo Time (UTE)-Based Methods for Magnetic Resonance Imaging of Peripheral Nerve

Shu-Juan Fan[1], **Jonathan Wong**[2], **Xin Cheng**[1,2], **Ya-Jun Ma**[1], **Eric Y. Chang**[1,2], **Jiang Du**[1], and **Sameer B. Shah**[2,3]

[1]Department of Radiology, University of California, San Diego, La Jolla, CA

[2]Research Service, Veterans Affairs San Diego Healthcare System, San Diego, CA

[3]Departments of Orthopaedic Surgery and Bioengineering, University of California, San Diego, La Jolla, CA

Abstract

Peripheral nerves are a composite tissue consisting of neurovascular elements packaged within a well-organized extracellular matrix. Their composition, size, and anatomy render nerves a challenging medical imaging target. In contrast to morphological magnetic resonance imaging (MRI), which represents the predominant approach to nerve imaging, quantitative MRI sequences can provide information regarding tissue composition. Here, we applied standard clinical CPMG and experimental 3D ultrashort echo time (UTE) Cones sequences for quantitative nerve imaging including T_2 measurement with single-component analysis, T_2* measurement with single-component and bi-component analyses, and magnetization transfer ratio (MTR) analysis. We demonstrated the feasibility and the high quality of single-component T_2*, bi-component T_2*, and MTR approaches to analyze nerves imaged with clinically deployed 3D UTE Cones pulse sequences. For 24 single fascicles from 8 nerves, we measured a mean single component T_2* of 22.6 ± 8.9 ms, and a short T_2* component with a mean T_2* of 1.7 ± 1.0 ms and a mean fraction of (6.74 ± 4.31)% in bi-component analysis. For 8 whole nerves, we measured a mean single component T_2* of 16.7 ± 2.2 ms, and a short T_2* component with a mean T2* of 3.0 ± 1.0 ms and a mean fraction of (15.56 ± 7.07)% in bi-component analysis. For 9 fascicles from 3 healthy nerves, we measured a mean MTR of (25.2 ± 1.9)% for single fascicles and a mean MTR of (23.6 ± 0.9)% for whole nerves. No statistically significant correlation was observed between any MRI parameter and routine histological outcomes, perhaps due to the small sample size and lack of apparent sample pathology. Overall, we have successfully demonstrated the feasibility of measuring quantitative MR outcomes *ex vivo*, which might reflect features of nerve structure and macromolecular content. These methods should be validated comprehensively on a larger and more diverse set of nerve samples, towards the interpretation of in vivo outcomes. These approaches have new and broad implications for the management of nerve disease, injury, and repair.

*Address for Correspondence: 9500 Gilman Drive, MC 0863, La Jolla, CA 92093, Phone: (858) 822-0720, sbshah@ucsd.edu.

Keywords

peripheral nerve; MRI; UTE; quantitative imaging

Introduction

Peripheral nerves are a composite tissue consisting of neurovascular elements packaged within a well-organized extracellular matrix. Endoneurial sheaths surround individual nerve fibers, which form parallel arrays with accompanying blood vessels and are fasciculated within the perineurium. The fascicles are bundled within the epineurium. Their composition, size, and anatomy render nerves a challenging medical imaging target.

Morphological imaging is the mainstay of current nerve imaging approaches. Clinical ultrasound may be used to identify epineurial borders and nerve shape[1], but suffers from limited contrast and resolution (0.2–0.5mm^2). Morphological magnetic resonance (MR) imaging, including newer three-dimensional (3D) and MR neurography sequences[3], capably identify epineurial, and sometimes perineurial, borders. However, these methods are usually qualitative, and observations of nerve signal intensity, size/shape, and structure each have their own set of limitations. Though nerves can be imaged with conventional clinical sequences, several important components of nerves are under-represented in the total signal and therefore underappreciated. This includes nerve collagen, which has a substantial contribution to structure and function. Collagen backbone protons are “invisible” with current MR imaging sequences[4]. Water protons are “visible” but the transverse relaxation time (T_2) is shortened due to the structure of collagen and its interactions with water[5]. In addition, the linear orientation and anisotropy of collagen within a nerve can affect signal intensity. Nerve signal can increase up to 175% as the overall orientation changes from parallel to 55° relative to the main magnetic field, termed the “magic angle effect”[6]. In fact, some nerves have been reported to display increased signal intensity in up to 60% of asymptomatic patients[7], highlighting the caution that must be used in interpreting such images. Overreliance on nerve size/shape can also be problematic since nerve size/shape are sensitive to joint configuration, and nerve deformation and flattening can be a normal part of joint movement[8]. Furthermore, evaluation of structure using conventional morphological MRI sequences is fundamentally limited by image resolution and acquisition time. With highly optimized conventional sequences focused on a very small field of view, resolution can approach 0.1 mm with 10–12 minute acquisition time, which is sufficient to resolve the perineurium of larger, more superficial nerves[9].

In contrast to morphological imaging approaches, quantitative MRI sequences can provide structural information on a submicron to micron scale – i.e., smaller than the highest achievable spatial resolution. For example, diffusion imaging is a very common technique in nerve imaging, and can provide quantitative information on the microenvironment of the nerve and enable tractography. Diffusion techniques are sensitive to nerve degeneration and regeneration[10,11]. However, most diffusion imaging techniques utilize echo times (TEs) in the range of 30–100 ms[10,11], and similar to other conventional sequences with longer TEs cannot provide information on the short T_2 components of nerve. Transverse relaxation

measurements, such as T_2[12] and T_2*[13], have also been used in peripheral nerve imaging, but again, the short T_2 components are not imaged when longer TEs are used. Furthermore, these measurements are exquisitely sensitive to magic angle effects, as noted above, confounding interpretation of quantitative values.

Recently, ultrashort time to echo (UTE) imaging with T_2* bi-component analysis has been used to quantify the signal contributions from the short and long relaxation components in multiple tissues[5]. In addition, UTE-magnetization transfer (MT) imaging has been used to provide quantitative information on the shortest T_2 components, including protons on the backbone of macromolecules such as collagen; such structures are not directly visible even with morphological UTE sequences[14]. Furthermore, MT measurements and bi-component fractions have been speculated to be less sensitive or insensitive to the magic angle effect[15–17]. In this study, we describe the application of standard clinical CPMG sequence for T_2 measurement and experimental 3D UTE Cones sequences for T_2* measurement with single- and bi-component analyses as well as MT ratio (MTR) analysis, which have previously been deployed in multiple tissues[5,14], to the imaging of peripheral nerves. Our primary goal was to demonstrate the feasibility and reliability of these methods for nerve imaging. We also performed preliminary correlations of UTE and UTE-MT outcomes with histological outcomes, as an initial effort to map imaging parameters to nerve structure.

Materials and Methods

Sample preparation

Fresh human tibial nerves at the tarsal tunnel were dissected from 8 donor lower limbs (donor age range = 20 – 92 years) that were obtained from tissue banks, as approved by institutional review board. Fresh-frozen tissue (i.e., no fixative) was acquired from the donor limbs and stored at −80°C for 6–12 months prior to being thawed for the first time at room temperature overnight. Nerves were dissected and stored within 1 hour at −20°C or imaged directly after equilibration to room temperature for 2–3 hours. The nerves were placed in perfluoropolyether (PFPE) (**Fomblin**® LC08; Solvay Inc.) in a 30-mL plastic syringe, and imaged with their long axis parallel to the main magnetic field. After MR imaging, nerves were fixed with 10% formalin, treated with 30% sucrose for cryoprotection, and cut to 10 μm-thick cross-sections prior to staining with routine hematoxylin and eosin (H&E). In addition, Masson’s trichrome staining was performed per product literature to identify connective tissue (Aniline blue component). The location of each histological section along the nerve was tracked, and matched to the corresponding MRI slice to allow correlation of imaging and histological outcomes in the same region.

MR imaging

All imaging experiments were performed on a 3T clinical MR scanner (GE Healthcare, Milwaukee, MI, USA) at room temperature (25°C) with peak gradient amplitude of 50 mT/m and maximum gradient slew rate of 200 mT/m/s. A home-made 22-mm diameter birdcage transit/receive coil was used for signal excitation and reception. Eight nerves were imaged in two sessions. In the first session, five nerves were imaged with CPMG and UTE sequences. In the second session, three nerves were imaged with UTE and UTE-MT

sequences. The integrity of all samples was assessed with histology. The latter three samples were used to correlate UTE or UTE-MT outcomes with histological outcomes.

A clinical CPMG sequence was performed (n = 5 nerves) using the following parameters: TR = 3000 ms, TEs = 14.7, 29.2, 44.1, 58.8, 73.6, 88.3, 102.9 and 117.7 ms, flip angle (FA) = 90°, field of view (FOV) = 20 × 20 mm^2, matrix size = 256 × 256, in-plane spatial resolution = 78 × 78 μm^2, slice thickness = 2 mm, no slice gap, and a total scan time of ~25 min. For T_2* measurements (n = 8), dual echo images were acquired using a 3D dual echo UTE Cones sequence which employed short radiofrequency (RF) rectangular pulses (duration = 78 μs) for signal excitation, followed by 3D spiral trajectories with conical view ordering[18]. The following parameters were used for T_2* measurements: repetition time (TR) = 200 ms, eight pairs of echo times (TEs), i.e., 0.032/13, 0.2/16, 0.4/19, 0.6/22, 0.8/25, 3/28, 6/31 and 9/34 ms, flip angle (FA) = 30°, FOV = 20 × 20 mm^2, matrix size = 256 × 256, in-plane spatial resolution = 78 × 78 μm^2, slice thickness = 1 mm, and 30 slices, scan time = ~35 min per acquisition (each pair of TEs).

For UTE-MT imaging (n = 3), a Fermi MT preparation pulse (duration, 8 ms; spectral bandwidth = 160 Hz) was added to the 3D UTE-Cones sequence. The following parameters were used: TR = 102 ms, TE = 32 μs, flip angle = 7°, field of view = 30 × 30 mm^2, slice thickness = 1.5 mm, and acquisition matrix = 320 × 320. A total of 12 sets of images were acquired with three different nominal flip angles of the MT pulse (300 °, 550 °, and 800°) in combination with four different off-resonance frequencies (2, 5, and 20 kHz). The total scan time was ~60 min.

Data analysis

ROIs were defined both on single fascicles and over a large area including several fascicles. The CPMG data were fitted offline to the following single component T_2 decay model in Matlab (Mathworks Inc. Natick, MA, USA),

$$S(TE) = S_0 \times e^{-TE/T2} + noise \quad [1]$$

where S_0 is the signal intensity at TE = 0.

The multi-TE UTE data were fitted offline to the following single component T_2* decay model (equation [2]), as well as to the following previously published bi-component fitting model (equation [3]) in Matlab:

$$S(TE) = S_0 \times e^{-TE/T2^*} + noise \quad [2]$$

$$S(TE) = A_S \times e^{-\frac{TE}{T2S^*}} + A_L \times e^{-\frac{TE}{T2L^*}} + noise \quad [3]$$

where S_0 is the signal intensity at TE = 0, $S(TE)$ is the UTE MR signal, A_S and A_L are the signal amplitudes of the short T_2* components (STCs) and long T_2* components (LTCs), T_{2S}* is the STC T_2*, and T_{2L}* is the LTC T_2*.

The MT ratio (MTR) is a commonly used semi-quantitative parameter in clinical applications of MT imaging[19]. MTR reflects the percentage attenuation of the steady-state MRI signal after the MT saturation pulse is applied[20]. In this study, MTR was calculated for each combination of different flip angles of the MT pulse and different off-resonance frequencies using the following equation[21]:

$$\mathrm{MTR} = (M_0 - M_{SAT})/M_0 \quad [4]$$

where M_0 is the equilibrium magnetization of the tissue, i.e. the magnitude of tissue signal on image acquired without off-resonance saturation, and M_{SAT} is the magnitude of tissue signal acquired with off-resonance saturation. The effects of off-resonance saturation pulse power and frequency offset on MTR were investigated systematically in this study.

Image processing

Image processing of histological sections was performed using MetaMorph software (Molecular Devices, Sunnyvale, CA). Digital images of nerves were captured from histology slides, and color thresholded to include regions positive for connective tissue. These thresholds were used to binarize the image. Area fractions within regions of interest were determined by manually outlining the intra-fascicular region (i.e., not including the connective tissue surrounding each fascicle, to match ROIs selected from MR data) or the intraepineurial region (including all fascicles, but excluding the outer epineurium), and calculating the percent of connective tissue-positive pixels within the ROI.

Results

We first imaged freshly harvested cadaveric tibial nerves using a standard clinical CPMG sequence (Figure 1). Results from a representative nerve reveal T_2 values of 28–33 ms for single fascicles (mean ± standard deviation, 31.2 ± 2.2 ms), and a T_2 value of 35 ms for a larger ROI covering the whole nerve, with an estimated fitting error of ±3 ms (Figure 1A–D). Single component fits of data from multi-TE images achieved $R^2 > 0.99$ for all datasets. Analysis of additional fascicular and whole nerve ROIs revealed similar T_2 values (Figure 1E).

We next investigated the feasibility and quality of T_2* measurements on tibial nerves imaged with the 3D UTE Cones pulse sequence. Images for a representative specimen are shown in Figure 2A. At TE of 0.032 ms both short T_2* and long T_2* components have strong signal, thus limiting contrast inside the nerve. Individual fascicles are more clearly visible in images with TE > 9 ms, presumably due to the decay of signals from short T_2 myelin sheaths and connective tissue in the perineurium and epineurium, and between fascicles. H&E staining images of the whole nerve (Figure 2B) and the single fascicle (Figure 2C, marked with a '*' in Fig. 2B) showed no visible signs of structural damage; this was similarly confirmed in all

the nerves included in this study. In addition, fascicular structure and organization was consistent along a length of 1mm (Figure 2D), suggesting that quantitative data within a voxel may be correlated with data from a histological section mapped within the voxel.

Analyses of single-component and bi-component fitting of multi-TE 3D UTE datasets were performed for fascicular and whole nerve ROIs from individual nerves. Analyses for two representative specimens are shown in Figures 3A–3D. Fits achieved $R^2 > 0.99$ for all datasets, but revealed variability in single-component (T_2*) and bi-component (T_{2S}*, T_{2L}*, f_S, f_L) parameters among individual fascicles as well as between individual fascicles and whole nerve ROIs. Averaged results from 24 individual fascicles and 8 whole nerve ROIs (3 individual fascicles per nerve) are shown in Figures 3E–3H. In all nerves, T_2* obtained with single component fitting was larger in fascicular ROI than in the whole nerve ROI (22.6 ± 8.9 ms vs. 16.7 ± 2.2 ms, Fig. 3H). Bi-component analyses revealed f_S and T_{2S}* of (6.74 ± 4.31) % and 1.7 ± 1.0 ms in individual fascicles vs. (15.56 ± 7.07)% and 3.0 ± 1.0 ms in whole nerve ROIs, respectively (Figs. 3E–3F). T_2* values obtained by single component analysis of 3D UTE data were intermediate to T_{2S}* and T_{2L}* values, but biased towards T_{2L}* values due to low f_S (Figs. 3F–3H).

We then tested the feasibility and quality of MTR on tibial nerves scanned with a 3D Cones UTE pulse sequence. 3D Cones UTE images without (M_0) and with MT contrast (M_{SAT}), and their subtraction images with varied flip angle of the MT pulse and off-resonance frequency are shown for a representative nerve (Figure 4A–C) from a 64-yr old male donor. For each specific flip angle used, the subtraction image showed higher signal-to-noise ratio when a lower off-resonance frequency was used. For each specific off-resonance frequency, the subtraction image showed higher signal-to-noise ratio when a larger flip angle was used. The highest MTR was obtained at the flip angle of 800° and the off-resonance frequency of 2 kHz. The MTR of three single fascicles was (23.8 ± 1.4)%, and that of the whole nerve was 22.6%. Figure 4D shows the average MTR of nine single fascicle ROIs and three large ROIs from three nerves. As compared with the T_2* measurements shown in Figure 3, MTR measurements appear to demonstrate smaller variances within and among different nerves, with single fascicle ROIs generally showing slightly larger MTR than large ROIs.

As a direct comparison between single-component, bi-component, and MTR analysis, we compared data from a pilot set of nerves analyzed with each method, and also processed histologically using H&E staining. The whole nerve appeared structurally normal on high-resolution histological images, and no microstructural difference was observed among the three single fascicles (Figures 5A–5B). Examination of both H&E and trichrome labeling confirmed the structural similarity of each fascicle (Figure 5B–E). Connective tissue positive area fractions calculated following binarization of intrafascicular regions 1, 2, and 3 from the trichrome labeled image were 38.3%, 25.2%, and 35.5% (Mean ± SEM: 33% ± 4%), respectively. For the large ROI (intraepineurial), the connective tissue positive area fraction was 39.6%. Despite this apparent similarity, large variations of the single-component T_2* values and bi-component T_{2L}* values were observed among the different single fascicle ROIs and between single fascicle ROIs and large ROIs (Figs. 5F–5G). However, very small variations were observed in bi-component T_{2S}* values for the three single fascicle ROIs and in MTR values for the four ROIs analyzed (Figs. 5G–5H). Linear regression analysis yielded

no significant correlation between any imaging parameter and connective tissue fraction (all $P > 0.05$, $R^2 < 0.2$). A summary of all quantitative analyses are presented in Table 1.

Discussion

We have described the implementation of standard clinical CPMG and new experimental 3D UTE Cones -based quantitative imaging techniques to assess the structure of peripheral nerves. We demonstrated the feasibility and the high quality of single-component T_2*, bi-component T_2*, and MTR approaches to analyze nerves imaged with 3D UTE Cones pulse sequences. We observed no statistically significant correlation between histological outcomes and any MRI parameters. Despite the apparent fascicular similarity within a given nerve (Figure 5), the single T2* (Figure 5F) and bi-component T2L* measurements (Figure 5G) fluctuated (Figure 1.2), while the MTR (Figure 5H) was relatively stable. The bi-component T2S* measurement was also relatively stable (Figure 5G), though its coefficient of variation was higher than that of MTR (standard deviation/mean in Table 1). These observations suggest that UTE-MTR measurements, and possibly bi-component UTE measurements, are more reliable than single component T2* measurements. We also speculate that MTR may be less sensitive to variability created by variations in nerve orientations relative to the main magnetic field (magic angle effect)[15–17]. Future studies will quantitatively evaluate this posited insensitivity of MTR to nerve orientation. Overall, we have successfully demonstrated the feasibility of imaging peripheral nerves with quantitative UTE MR methods.

Quantitative MRI of nerves

The focus of this work was on the feasibility of imaging short T_2 components (such as collagen and myelin) that are typically “invisible” when using conventional imaging techniques[22], using UTE sequences that enable the detection of signal in short T_2* tissues/tissue components, and quantification of structural elements within these tissues[5]. Morphological and quantitative UTE-MRI sequences have been applied to many short T_2 tissues and components, including cartilage, menisci, bone, tendons, and myelin in the central nervous system[5,23–25]. This study represents the application of such methods to a new target -- peripheral nerves.

Previous nerve MR studies have largely focused on improving nerve visualization, which typically involves improving contrast between epineurial or fascicular boundaries of nerve and the surrounding structures. Recent studies have also used diffusion tensor MR imaging as initial efforts in quantitative imaging of nerves[10,11]. While these approaches successfully distinguish between changes in nerve fiber continuity[26–29], the interpretation of such studies is not trivial, as assumptions are often made as to what tissue structures contribute to diffusion signal. For example, diffusion in nerves is often interpreted to reflect movement of water within axons[29,30]. However, changes in diffusion parameters do not appear to strongly correlate with axon number or size, a fact that may reflect the relatively small percentage of nerve volume occupied by axons, in comparison to myelin, the basal lamina, and extracellular matrix[29]. Such findings reflect a need to more rigorously correlate imaging

outcomes with histological measures as well as to develop imaging approaches yielding signatures of specific biological components.

In our study, we correlated UTE outcomes, whose signatures have been attributed to macromolecules such as collagen[4], with histological measures of connective tissue content. Bi-component analysis provided significant insight into the structural characteristics of nerve. Particularly compelling was the fact that short fractions were reasonably conserved across multiple fascicles within a nerve. However, compared to area fractions of connective tissue quantified histologically (Figure 5), these fractions were quite low by percentage, suggesting that collagen, myelin, and other macromolecules exist within a highly aqueous environment. Further examination of ROIs in peri-fascicular regions (i.e., perineurium and epineurium), which were not included in this study, are posited to be more enriched in short fraction, perhaps reflecting an increase in collagen relative to water. This may reflect tighter packing of collagen in the perinerium vs. endoneurium, and thus restricted water content as well.

Scan times and clinical translation

Most recently we have focused our efforts on efficiency in order to decrease scan times. The 3D-UTE-Cones sequence is the result of these efforts[31], which can allow clinical imaging of the nerves within the forearm within a few minutes. In this study, pulse sequences for MT imaging took 5 min per data point with a certain MT power and frequency offset; T_2* bi-component analysis took 280 min for 16 data points. These are not practical for clinical translation, however, ultimately a sensitivity analysis on each modeling approach will provide a better understanding of a minimum number and range of data points that provide more accurate parameters. Furthermore, the total scan time can be greatly reduced by using lower in-plane resolution, thicker (and thus fewer) slices, and less spatial coverage. Our recent study on the same clinical system suggests that bi-component analysis may be completed in less than eight minutes, while each MT measurement (for a certain MT power and frequency offset) may be completed in less than one minute with a typical SNR of 10–40 depending on the size of the coil, and MT modeling may be completed in less than ten minutes[32]. These time frames are reasonable for clinical translation.

Limitations

Our data must be interpreted in the context of several limitations to our work. First, we performed analysis on freeze-thawed cadaveric nerves. While there were no visual indicators of freeze damage to any of the imaged specimens, based on histological assessment of the integrity of epineurial, perineurial, and intrafascicular compartments, there may be more subtle artifacts associated with freeze-thaw damage (e.g., to cell membranes) or differences *in vivo* vs. *ex vivo* (e.g., intra-nerve pressure, hydration, or temperature) that could influence imaging outcomes. Also, while we inspected nerves for gross structural changes, we were blinded to any pertinent medical history that may have influenced nerve quality. Additionally, there was a reduction in data quality and an increase in challenges associated with image registration with smaller ROIs. While we were able to successfully generate T_2*, fraction and MTR values from individual fascicles, we were unable to compare ROIs of sub-fascicular or peri-fascicular scales. There are also several limitations related to correlation of

imaging outcomes with histology. While we matched the orientation and location of each histology section with a corresponding MRI slice, there are resolution differences between the two modalities and differences in section and slice thickness. Also, there was mild distortion of the sample during MR scanning due to its embedding; this resulted in slight differences in shape between fascicles/nerve in MR images vs. histological images. For these reasons, our minimum ROI was a single fascicle (i.e., no sub-fascicular ROI, for which the above differences might preclude an accurate comparison). Finally, we emphasize that any correlation between MR and histological outcomes should be viewed as preliminary; a comprehensive correlation will likely require the examination of pathological specimens, to broaden the range of structural outcomes.

Conclusion

We have demonstrated the feasibility of applying quantitative MRI methods to peripheral nerves *ex vivo*. There is considerable clinical value in the development and validation of new MR methodologies to quantify changes in nerve morphology. Beyond the identification of fascicular or nerve boundaries, the ability to measure changes in collagen quantity, localization, or organization has significant value for any number of neuropathies or injuries in which nerve structure is altered. Such approaches have new and broad implications for the management of disease, including the assessment of the extent of nerve injury or regeneration (i.e., fascicular continuity, identification of fibrosis, or identification of a regenerating nerve front), surgical planning or pre-operative decision making, and development or assessment of new strategies for physical therapy, surgery, and rehabilitation.

Acknowledgments

The authors acknowledge grant support from the NIH (1R01 NS092650), American Foundation for Surgery of the Hand (Award #1242), and the Department of Veterans Affairs (1I21 RX002367).

Abbreviations

2D	two-dimensional
3D	three-dimensional
FA	flip angle
FOV	field of view
H&E	hematoxylin and eosin
MRI	magnetic resonance imaging
MT	Magnetization Transfer
MTR	magnetization transfer ratio
PFPE	perfluoropolyether
RF	radiofrequency

ROI	region of interest
T2	transverse relaxation time
TE	echo time
TR	repetition time
UTE	ultrashort echo time

References

1. Lawande AD, Warrier SS, Joshi MS. Role of ultrasound in evaluation of peripheral nerves. Indian J Radiol Imaging. 2014; 24(3):254–258. [PubMed: 25114388]
2. Moran CM, Pye SD, Ellis W, et al. A comparison of the imaging performance of high resolution ultrasound scanners for preclinical imaging. Ultrasound Med Biol. 2011; 37(3):493–501. [PubMed: 21256667]
3. Amrami KK, Felmlee JP, Spinner RJ. MRI of peripheral nerves. Neurosurg Clin N Am. 2008; 19(4): 559–572. [PubMed: 19010281]
4. Ma YJ, Chang EY, Bydder GM, Du J. Can ultrashort-TE (UTE) MRI sequences on a 3-T clinical scanner detect signal directly from collagen protons: freeze-dry and D2O exchange studies of cortical bone and Achilles tendon specimens. NMR Biomed. 2016; 29(7):912–917. [PubMed: 27148693]
5. Chang EY, Du J, Chung CB. UTE imaging in the musculoskeletal system. J Magn Reson Imaging. 2015; 41(4):870–883. [PubMed: 25045018]
6. Chappell KE, Robson MD, Stonebridge-Foster A, et al. Magic angle effects in MR neurography. AJNR Am J Neuroradiol. 2004; 25(3):431–440. [PubMed: 15037469]
7. Husarik DB, Saupe N, Pfirrmann CW, Jost B, Hodler J, Zanetti M. Elbow nerves: MR findings in 60 asymptomatic subjects--normal anatomy, variants, and pitfalls. Radiology. 2009; 252(1):148–156. [PubMed: 19451541]
8. Goetz JE, Kunze NM, Main EK, et al. MRI-apparent localized deformation of the median nerve within the carpal tunnel during functional hand loading. Ann Biomed Eng. 2013; 41(10):2099–2108. [PubMed: 23612911]
9. Felisaz PF, Chang EY, Carne I, et al. In Vivo MR Microneurography of the Tibial and Common Peroneal Nerves. Radiol Res Pract. 2014; 2014:780964. [PubMed: 25548670]
10. Lehmann HC, Zhang J, Mori S, Sheikh KA. Diffusion tensor imaging to assess axonal regeneration in peripheral nerves. Exp Neurol. 2010; 223(1):238–244. [PubMed: 19879260]
11. Sun C, Hou Z, Hong G, Wan Q, Li X. In vivo evaluation of sciatic nerve crush injury using diffusion tensor imaging: correlation with nerve function and histology. J Comput Assist Tomogr. 2014; 38(5):790–796. [PubMed: 24943253]
12. Shen J, Zhou CP, Zhong XM, et al. MR neurography: T1 and T2 measurements in acute peripheral nerve traction injury in rabbits. Radiology. 2010; 254(3):729–738. [PubMed: 20177088]
13. Tagliafico A, Bignotti B, Tagliafico G, Martinoli C. Peripheral nerve MRI: precision and reproducibility of T2*-derived measurements at 3.0-T : a feasibility study. Skeletal Radiol. 2015; 44(5):679–686. [PubMed: 25631357]
14. Chang EY, Bae WC, Shao H, et al. Ultrashort echo time magnetization transfer (UTE-MT) imaging of cortical bone. NMR Biomed. 2015; 28(7):873–880. [PubMed: 25981914]
15. Shao H, Chang EY, Pauli C, et al. UTE bi-component analysis of T2* relaxation in articular cartilage. Osteoarthritis Cartilage. 2016; 24(2):364–373. [PubMed: 26382110]
16. Pauli C, Bae WC, Lee M, et al. Ultrashort-echo time MR imaging of the patella with bicomponent analysis: correlation with histopathologic and polarized light microscopic findings. Radiology. 2012; 264(2):484–493. [PubMed: 22653187]
17. Henkelman RM, Stanisz GJ, Kim JK, Bronskill MJ. Anisotropy of NMR properties of tissues. Magn Reson Med. 1994; 32(5):592–601. [PubMed: 7808260]

18. Ma YJ, Chang EY, Carl M, Du J. Quantitative magnetization transfer ultrashort echo time imaging using a time-efficient 3D multispoke Cones sequence. Magn Reson Med. 2017
19. Helms G, Dathe H, Dechent P. Modeling the influence of TR and excitation flip angle on the magnetization transfer ratio (MTR) in human brain obtained from 3D spoiled gradient echo MRI. Magn Reson Med. 2010; 64(1):177–185. [PubMed: 20572139]
20. Dousset V, Grossman RI, Ramer KN, et al. Experimental allergic encephalomyelitis and multiple sclerosis: lesion characterization with magnetization transfer imaging. Radiology. 1992; 182(2): 483–491. [PubMed: 1732968]
21. Henkelman RM, Stanisz GJ, Graham SJ. Magnetization transfer in MRI: a review. NMR Biomed. 2001; 14(2):57–64. [PubMed: 11320533]
22. Horch RA, Gore JC, Does MD. Origins of the ultrashort-T2 1H NMR signals in myelinated nerve: a direct measure of myelin content? Magn Reson Med. 2011; 66(1):24–31. [PubMed: 21574183]
23. Du J, Carl M, Bydder M, Takahashi A, Chung CB, Bydder GM. Qualitative and quantitative ultrashort echo time (UTE) imaging of cortical bone. J Magn Reson. 2010; 207(2):304–311. [PubMed: 20980179]
24. Du J, Carl M, Diaz E, et al. Ultrashort TE T1rho (UTE T1rho) imaging of the Achilles tendon and meniscus. Magn Reson Med. 2010; 64(3):834–842. [PubMed: 20535810]
25. Sheth V, Shao H, Chen J, et al. Magnetic resonance imaging of myelin using ultrashort Echo time (UTE) pulse sequences: Phantom, specimen, volunteer and multiple sclerosis patient studies. Neuroimage. 2016
26. Haakma W, Jongbloed BA, Froeling M, et al. MRI shows thickening and altered diffusion in the median and ulnar nerves in multifocal motor neuropathy. Eur Radiol. 2017; 27(5):2216–2224. [PubMed: 27655303]
27. Heckel A, Weiler M, Xia A, et al. Peripheral Nerve Diffusion Tensor Imaging: Assessment of Axon and Myelin Sheath Integrity. PLoS One. 2015; 10(6):e0130833. [PubMed: 26114630]
28. Gallagher TA, Simon NG, Kliot M. Diffusion tensor imaging to visualize axons in the setting of nerve injury and recovery. Neurosurg Focus. 2015; 39(3):E10.
29. Boyer RB, Kelm ND, Riley DC, et al. 4.7-T diffusion tensor imaging of acute traumatic peripheral nerve injury. Neurosurg Focus. 2015; 39(3):E9.
30. Takagi T, Nakamura M, Yamada M, et al. Visualization of peripheral nerve degeneration and regeneration: monitoring with diffusion tensor tractography. Neuroimage. 2009; 44(3):884–892. [PubMed: 18948210]
31. Carl M, Bydder GM, Du J. UTE imaging with simultaneous water and fat signal suppression using a time-efficient multispoke inversion recovery pulse sequence. Magn Reson Med. 2015
32. Ma YJ, Chang EY, Carl M, Du J. Quantitative magnetization transfer ultrashort echo time imaging using a time-efficient 3D multispoke Cones sequence. Magn Reson Med. 2018; 79(2):692–700. [PubMed: 28470838]

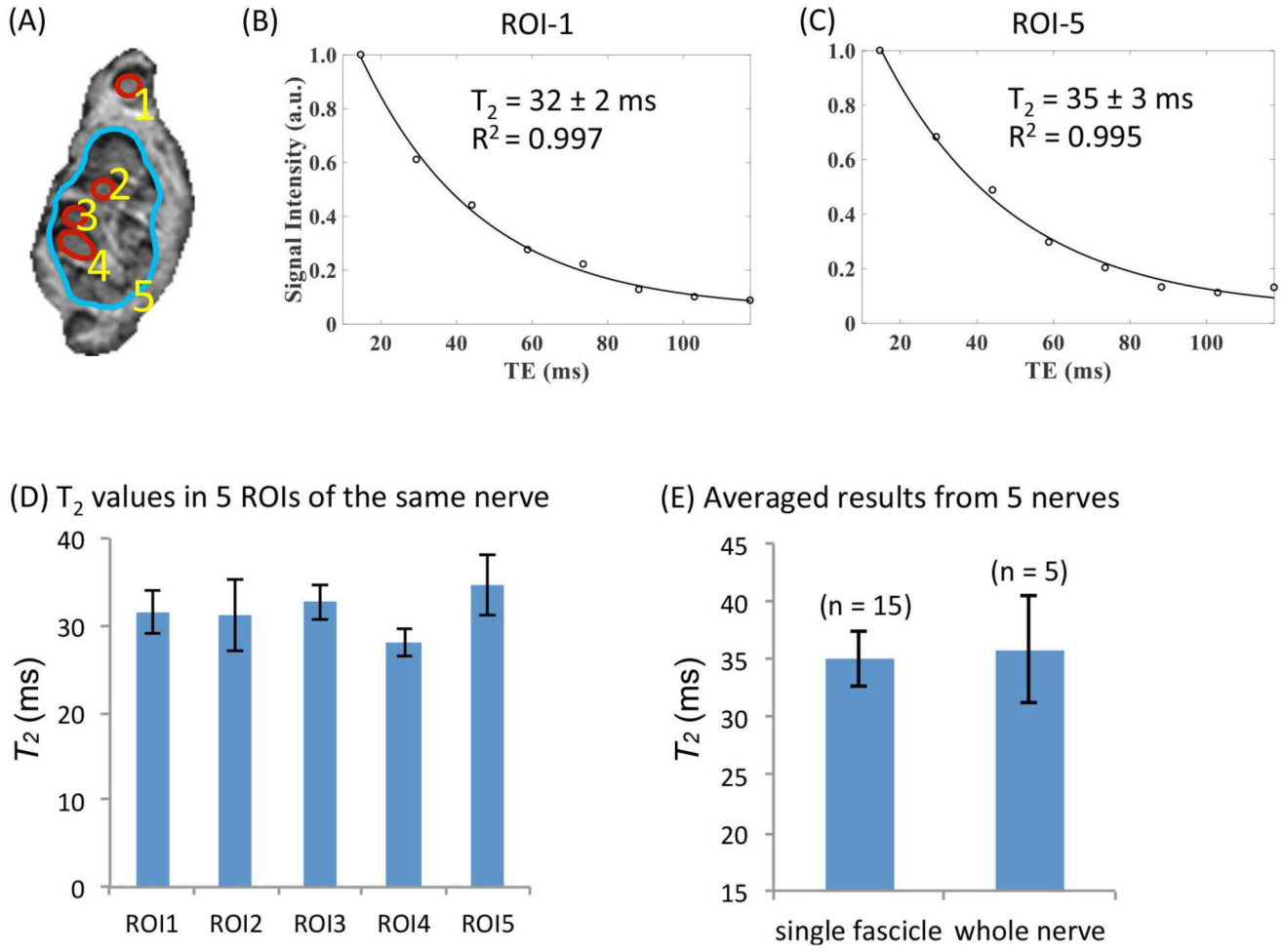

Figure 1.

Single-component T_2 measurements using a clinical CPMG sequence with TEs = 14.7, 29.2, 44.1, 58.8, 73.6, 88.3, 102.9 and 117.7 ms. **(A)** Illustration of the definitions of single-fascicle ROIs and large-ROIs (CPMG, TE = 14.7 ms). **(B)** Representative T_2 fitting result in a single-fascicle ROI (ROI1 as shown in Fig. A) and a large ROI (ROI5 as shown in Fig. A). **(C)** T_2 values measured from the five ROIs defined in **(A)**. (D) Average T_2 values measured from 15 single-fascicle ROIs and 5 large ROIs (i.e., 3 single-fascicle ROIs and one large ROI from each nerve. Five nerves were measured in total.)

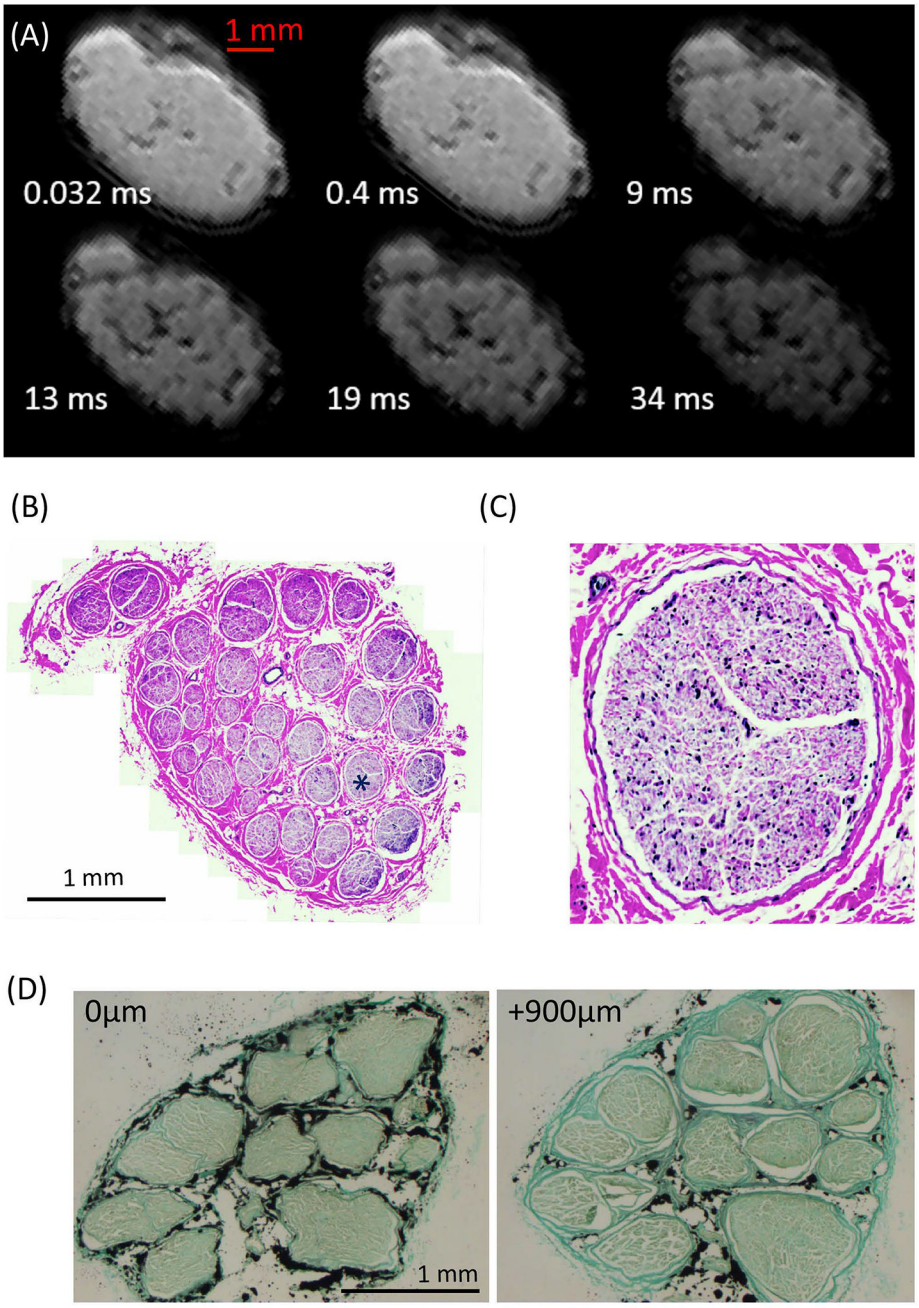

Figure 2.

(A) 3D Cones UTE images of one representative nerve with TEs marked on each image. **(B–C)** H&E staining images of the whole nerve **(B)** and a single fascicle **(C**, as marked with a '*' in **(B))**. **(D)** H&E staining of two slices ~1mm apart show similar fascicular organization and structure, indicating the validity of mapping histological outcomes from histological ROIs to MR ROIs.

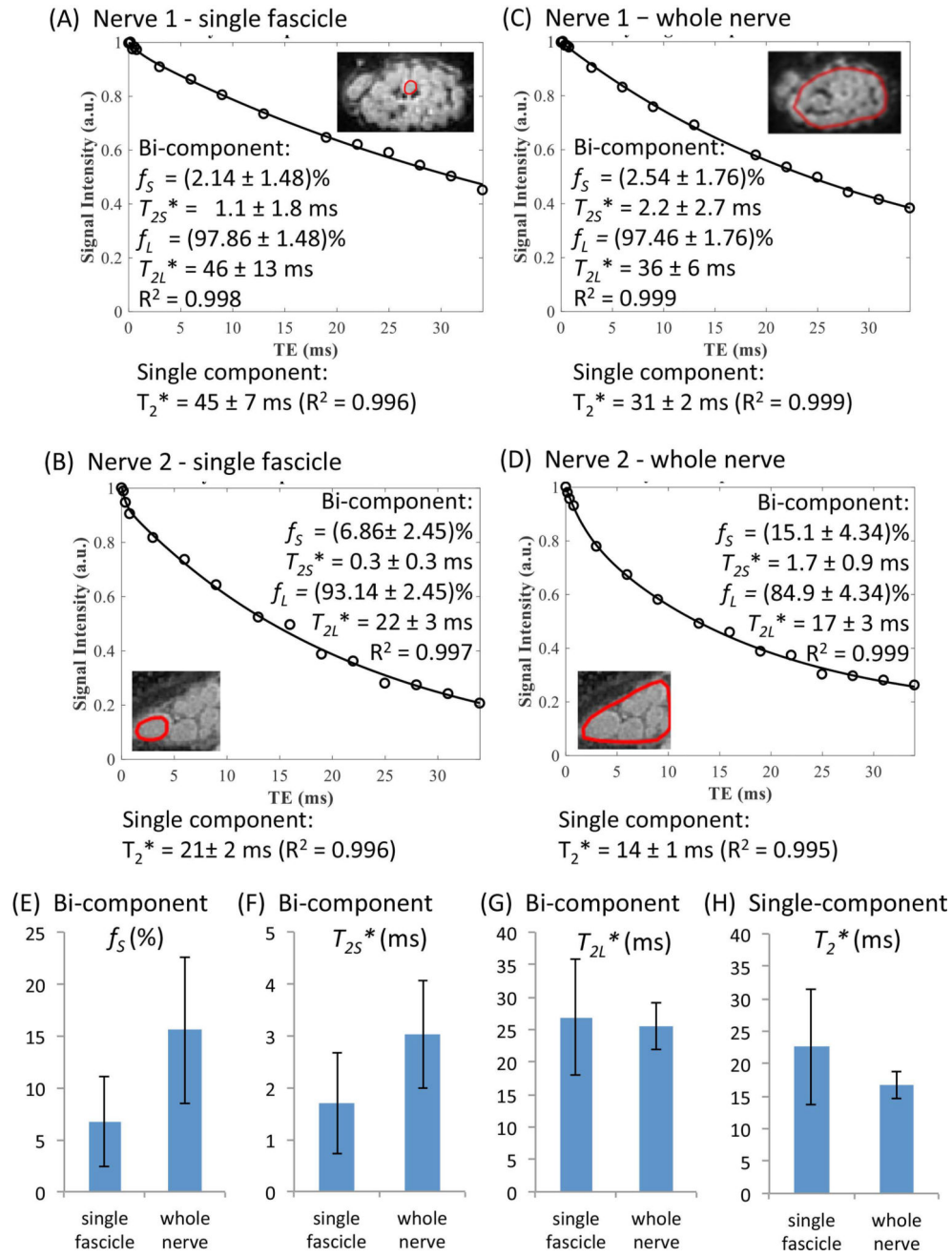

Figure 3.

(A–D) Bi-component and single component T2* fitting results of two single fascicles (A, C) and two whole nerves which include these fascicles (B, D). (E–H) UTE bi-component T2* fitting and single component T2* fitting results from eight nerves. Totally 24 fascicles from 8 nerves were analyzed. fS, fraction of short T2* components (STCs); T2S*, T2* of the STCs; T2L*, T2*of the long T2* components.

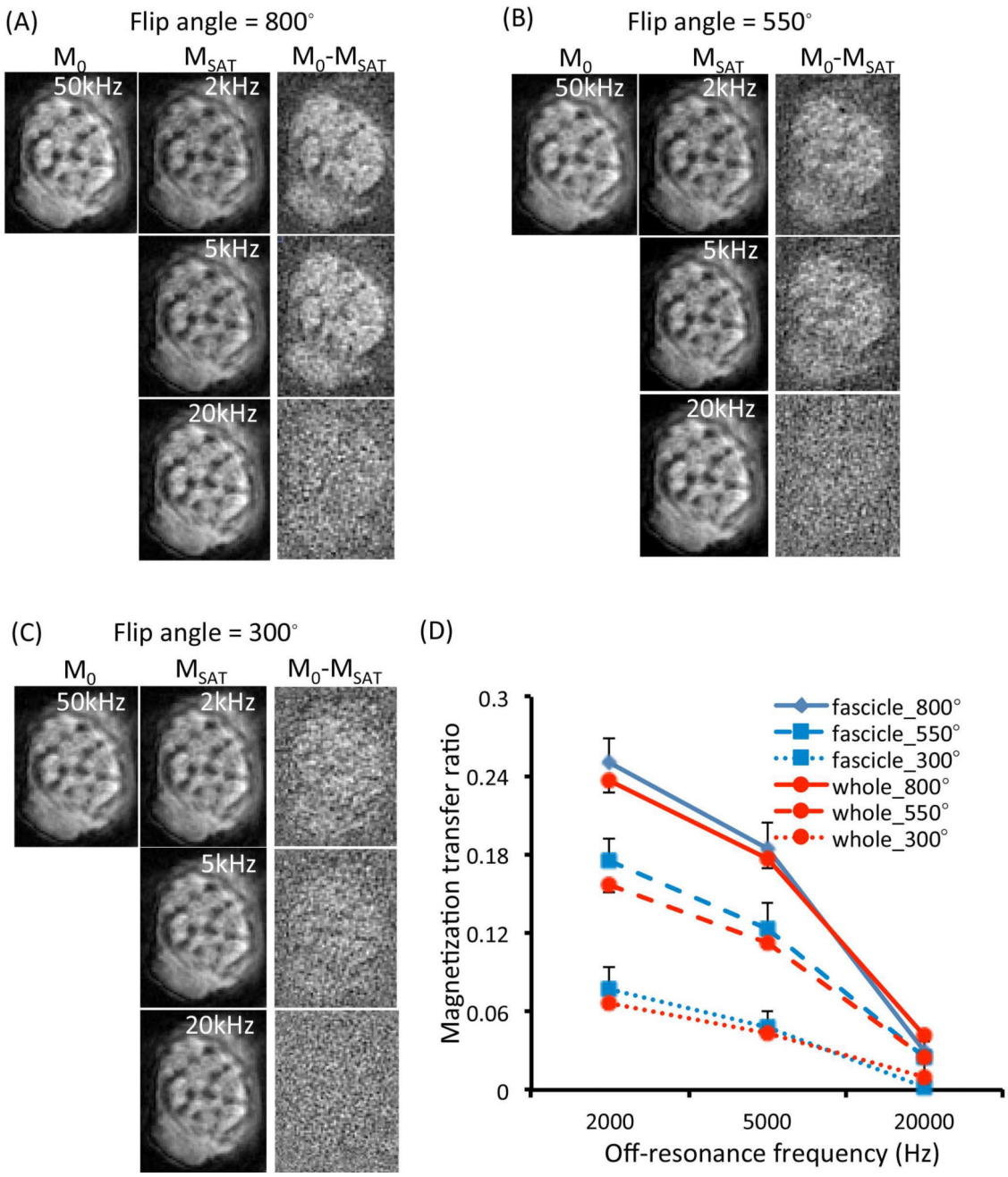

Figure 4.

(A–C) UTE images without (M_0) and with MT contrast (M_{SAT}), and their subtraction images ($M_0 - M_{SAT}$) obtained from a 64-yr old male donor using different flip angles of the MT pulse and different off-resonance frequencies. Higher signal-to-noise ratio in the subtraction image suggests higher MTR. **(D)** Mean MTR values of single fascicle ROIs (n = 9) and whole nerve ROIs (n = 3) plotted against the off-resonance frequency used and different flip angles of the MT pulse (left). Error bars reflect standard deviations.

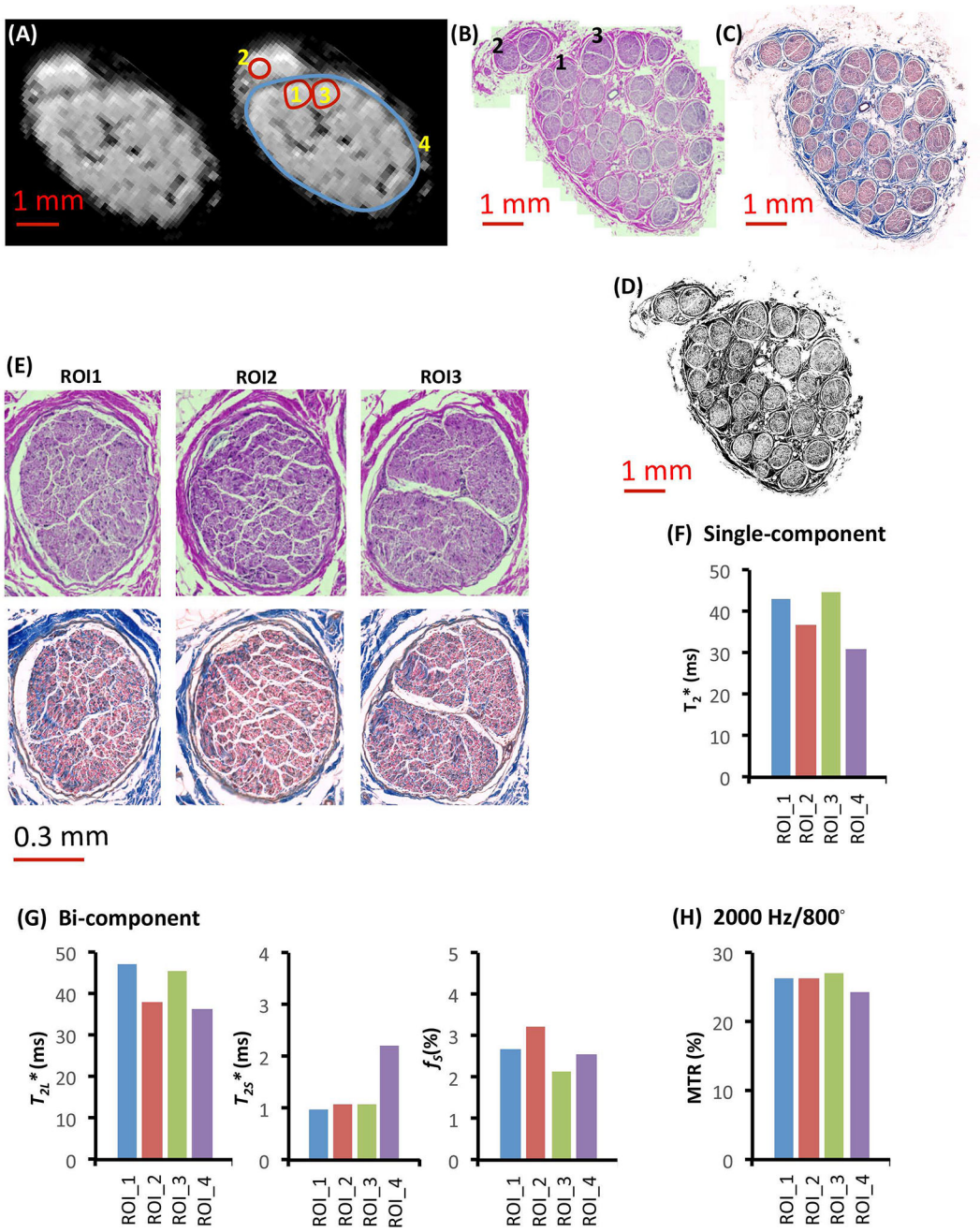

Figure 5.

Histological images and MR parameters of tibial nerve from a 38-yr old female donor. **(A–C)** Definitions of regions of interest on **(A)** the MR image, **(B)** corresponding H&E labeled image, and **(C)** trichrome labeled image. **(D)** Thresholded (binarized) image with connective tissue-positive pixels in black. **(E)** High resolution histological images of three single fascicles labeled with H&E (top row, gross structure) or trichrome (bottom row, specific for connective tissue) staining. **(F)** Single-component T_2* fitting results in four ROIs. **(G)** Bi-

component T_2* fitting results in four ROIs. **(H)** MTR values measured from four ROIs with an off-resonance frequency of 2000 Hz and an MT pulse flip angle of 800°.

Table 1

Summary of the quantitative analyses. 15 fascicles from 5 nerves were analyzed for CPMG. 24 fascicles from 8 nerves were analyzed for Cones UTE data, of which 9 fascicles from 3 nerves were also analyzed for MTR and histological connective tissue quantification. Data were presented as Mean ± Standard deviation.

	CPMG Single component T2 (ms) (n = 5)	Cones UTE Single component T2* (ms) (n = 8)	Cones UTE Bi-component fitting (n = 8)			MTR (%) (2000 Hz/800°) (n = 3)	Connective Tissue % (n = 3)
			f_S (%)	T_{2S}* (ms)	T_{2L}* (ms)		
Single fascicle ROI	35.4 ± 4.7	22.6 ± 8.9	6.74 ± 4.31	1.7 ± 1.0	26.7 ± 9.0	25.2 ± 1.9	30.0 ± 12.1
Large ROI	36.6 ± 4.6	16.7 ± 2.2	15.56 ± 7.07	3.0 ± 1.0	25.5 ± 3.6	23.6 ± 0.9	N/A